Supplement of Atmos. Chem. Phys. Discuss., 15, 28815–28866, 2015
http://www.atmos-chem-phys-discuss.net/15/28815/2015/
doi:10.5194/acpd-15-28815-2015-supplement

Atmospheric Chemistry and Physics Discussions

Supplement of

Direct measurements of OH and other product yields from the HO_2 + $CH_3C(O)O_2$ reaction

F. A. F. Winiberg et al.

Correspondence to: P. W. Seakins (p.w.seakins@leeds.ac.uk)

Contents

S1. Characterisation of HIRAC lamps

Semi-quantitative measurements of the lamp emission spectra and intensity as a function of time for the warm up period were measured using a 2Π quartz diffuser spectral radiometer (SpecRad) which was coupled to a fixed grating spectrometer (Ocean Optics, QE65000Pro) *via* a fibre optic cable. The spectrometer was calibrated to operate over the 250 - 750 nm range at < 1 nm resolution with light detected on a cooled, fast Fourier transform charge-coupled device (FFT-CCD, Hamamatsu). The SpecRad diffuser dome was introduced into the KF-40 opening of an ISO-500 flange at the side of the chamber. The chamber was over-pressurised with N_2 (laboratory supply), flowing gas out past the SpecRad diffuser which was not vacuum sealed to the chamber. This ensured removal of photolabile species that could potentially interfere with the light intensity measurements. Spectra were integrated over 100 ms; 10 spectra were averaged to achieve a 1 s time resolution using the supplied SpectraSuite software. After initiating data recording, the lamps were switched on and spectra were recorded for ~30 minutes. The emission time profile was calculated by integrating each spectrum between the 350 - 400 nm range. At room temperature (293 K), the lamps were observed to have a warm up period, reaching maximum output at ~150 s, before decreasing at longer times due to the optimum temperature being passed. The stable lamp emission at longer times was assumed to be equal to the overall photolysis rate in the chamber, therefore the emission time profile was used to constrain the chlorine photolysis rate when performing the chemical modelling.

S2. Experimental Data

S2.1 Examples of Addition HOx Profiles

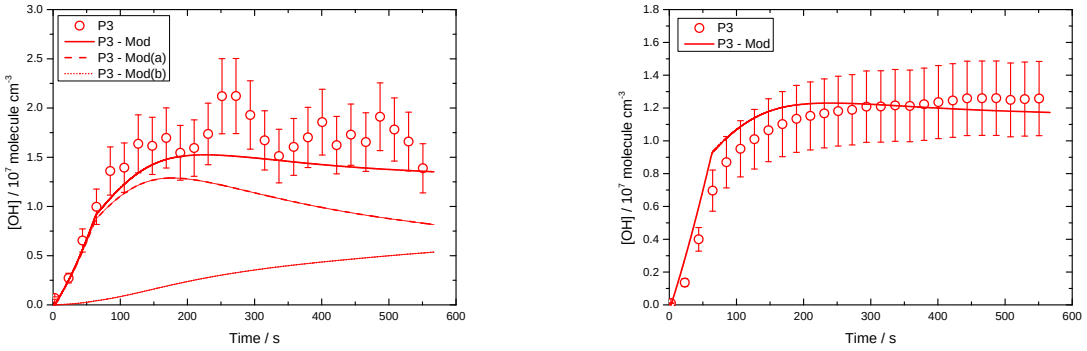

Fig. S1. The OH and HO_2 time profiles for experiment P3 at $[CH_3OH]_0$:$[CH_3CHO]_0 \approx 4$, 1000 mbar in air and 293 K. Chemical model predictions also shown (P3:Model) calculated using optimised branching ratios $\alpha_{5c} = 0.56 \pm 0.09$ calculated using the fitted $k_{5c} = 2.4 \times 10^{-11}$ cm^3 $molecule^{-1}$ s^{-1}. Contribution to total [OH] from reaction R5c and all other secondary sources are shown in Model(a) and Model(b) traces respectively. Error bars represent uncertainty to ± 1σ in the FAGE calibration procedure.

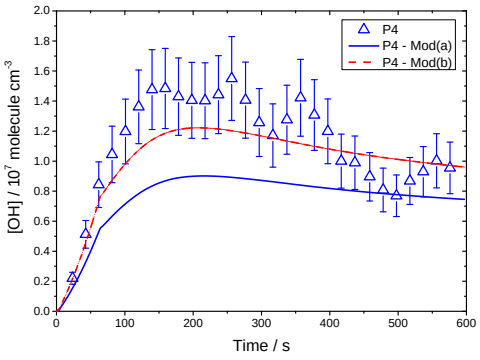

Fig. S2. The OH time profiles for experiment P4 at $[CH_3OH]_0$:$[CH_3CHO]_0 \approx 4$, 1000 mbar in air and 293 K. Compared to P3, the photolysis rate is higher, but because $[Cl_2]$ is lower, the peak [Cl] is lower than P3 and correspondingly peak OH is lower. Chemical model predictions also shown (P4:Model b) calculated using optimised branching ratios $\alpha_{5c} = 0.58$ calculated using the fitted $k_{5c} = 2.4 \times 10^{-11}$ cm^3 $molecule^{-1}$ s^{-1}. Error bars represent uncertainty to ± 1σ in the FAGE calibration procedure.

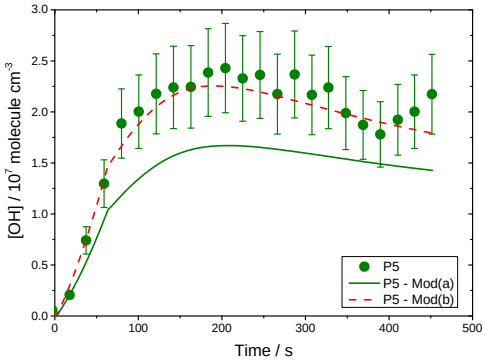

Fig. S3. The OH time profiles for experiment P5 at $[CH_3OH]_0$:$[CH_3CHO]_0 \approx 4$, 1000 mbar in air and 293 K. Compared to P3, the photolysis rate is higher (8 lamps), and although $[Cl_2]$ is lower, the peak [Cl] is higher than P3 and correspondingly peak OH is higher. Chemical model predictions also shown (P5:Model b) calculated using optimised branching ratios $\alpha_{5c} = 0.55$ calculated using the fitted $k_{5c} = 2.4 \times 10^{-11}$ cm^3 molecule^{-1} s^{-1}. Error bars represent uncertainty to ± 1σ in the FAGE calibration procedure.

S2.2 Additional Data on P 2 (see Fig. 5 in main text)

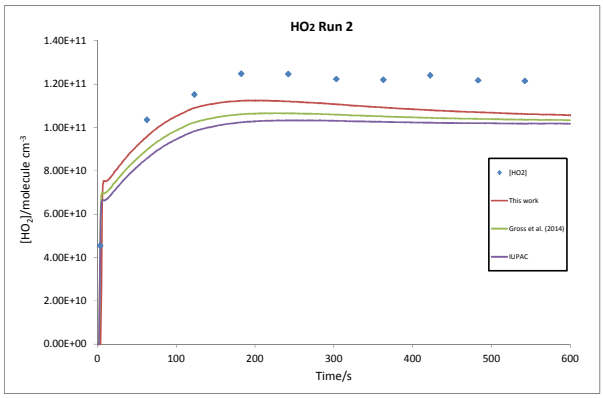

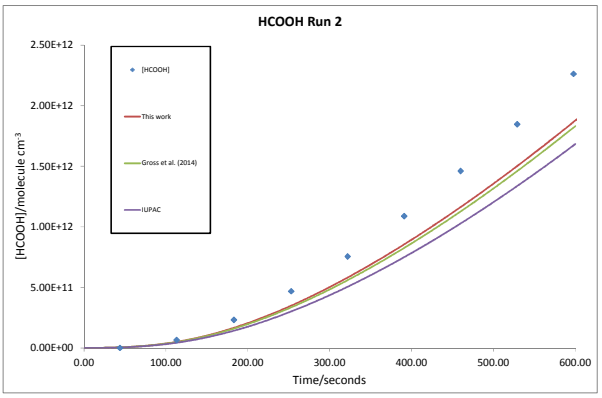

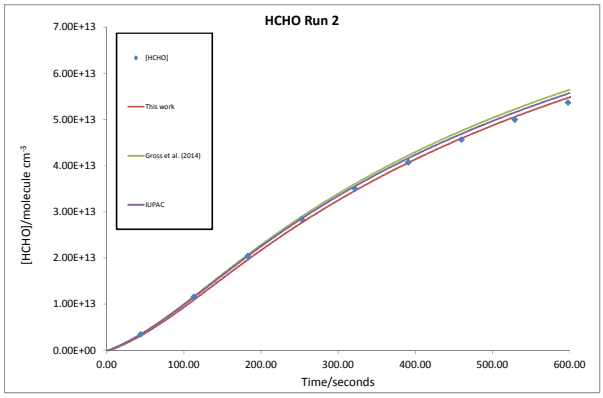

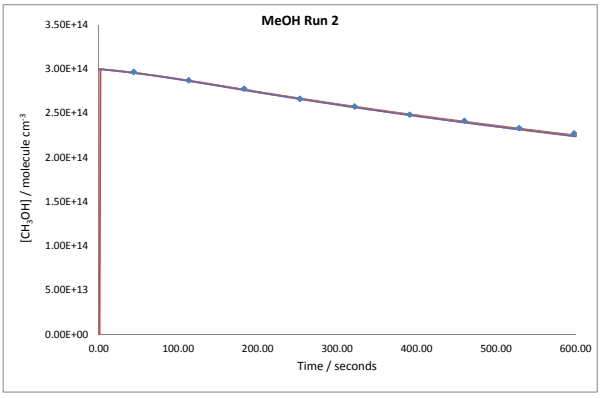

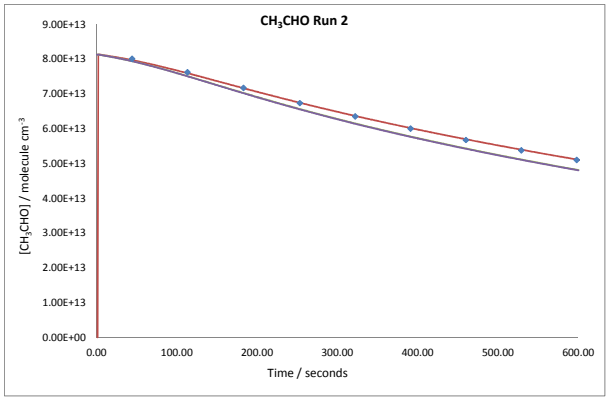

Fig. S4. Examples of data and fits from experiment P2. Errors not shown, but typically 10%.

S2.3 Examples of Additional Data from Experiment P11

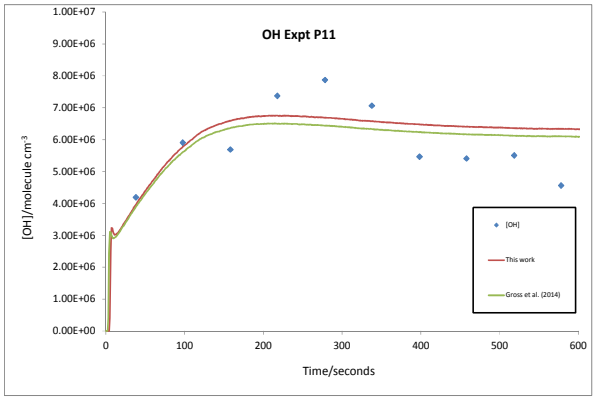

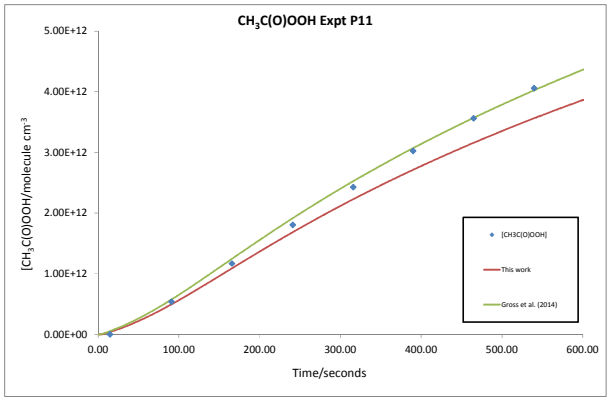

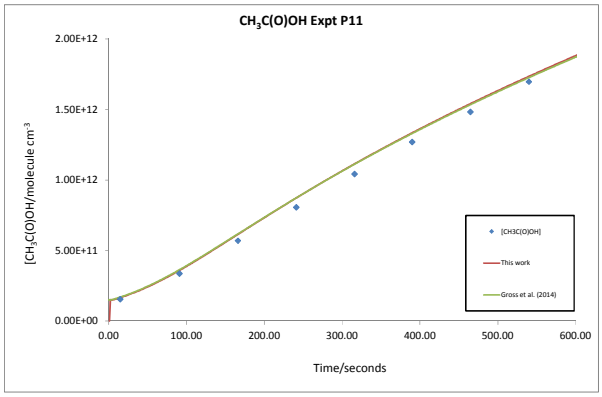

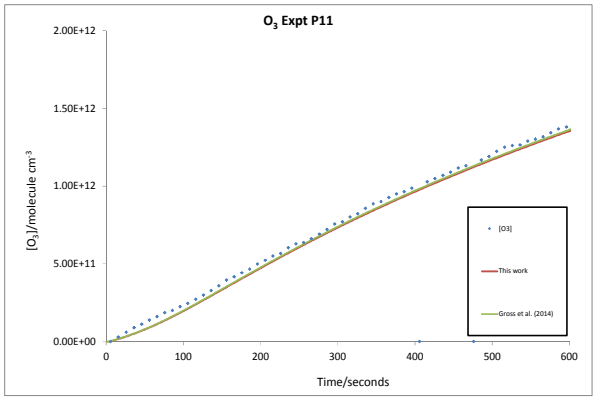

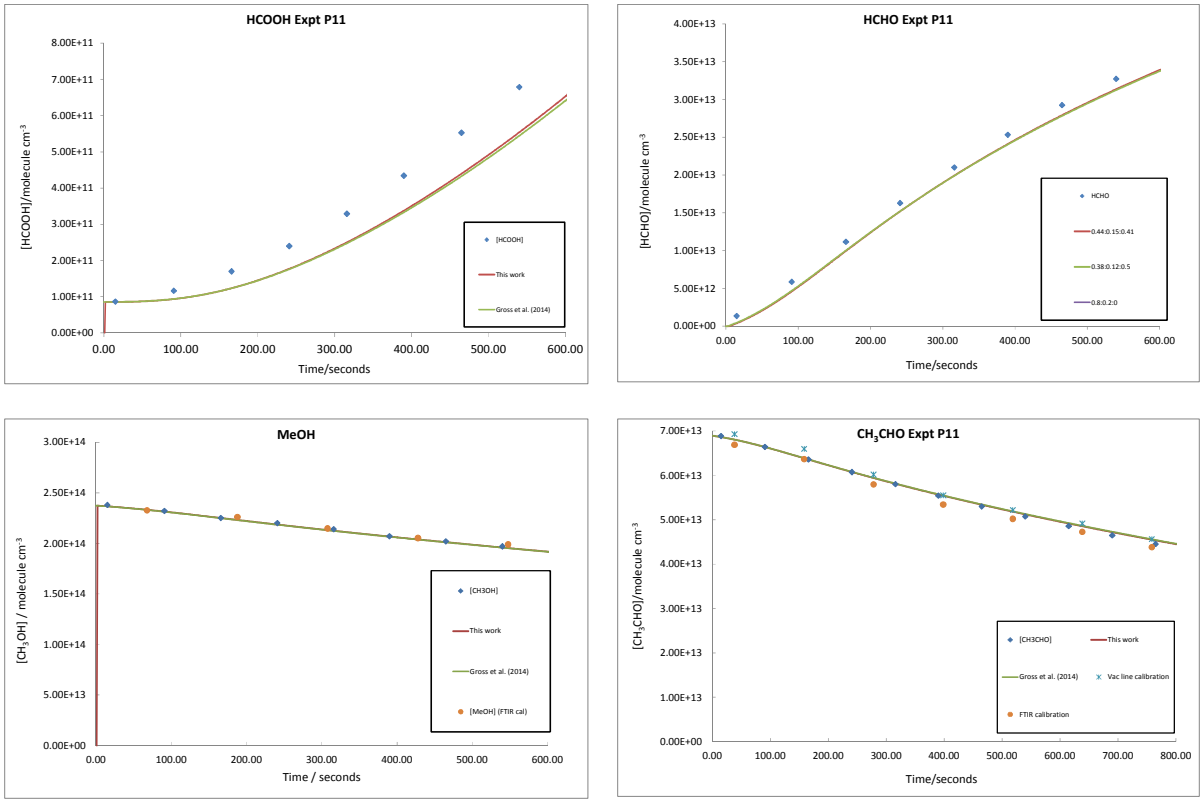

Fig. S5. Examples of data from Expt P11. For the acetaldehyde plot, data based on two different calibration methods are presented showing excellent agreement between the two methods.

S3. Investigations into possible interferences

IR cross sections for both $CH_3C(O)OOH$ and $CH_3C(O)OH$ used in this investigation were determined using the HIRAC FTIR equipped with a multipass cell. The measurement of $CH_3C(O)OOH$ was completed in-line with the method described by Orlando et al. (2000) and was within uncertainty of the cross-section presented therein. This method was non-trivial, requiring very accurate gas handling of very small volumes (~20 µl) of 40% $CH_3C(O)OOH$ in $CH_3C(O)OH$, followed by subtraction of the $CH_3C(O)OH$ spectrum. Hence there was a larger fractional uncertainty in the absolute measured $CH_3C(O)OOH$ compared to other IR active species (±0.2 vs ± 0.1). Furthermore, during experiments, the concentrations of $CH_3C(O)OOH$ and $CH_3C(O)OH$ were extracted from the carbonyl region of the MIR spectrum (~1700 cm^{-1}) using a non-linear least squares based fitting algorithm. This relied upon the deconvolution of overlapping absorptions from six well-characterised species ($CH_3C(O)OOH$, $CH_3C(O)OH$, HCHO, HCOOH, CH_3OH and CH_3CHO), and hence the

introduction of an unknown absorption would lead to an over- or underestimation of the concentrations for all species determined using this fitting method. In a blind test the software was found to be in excellent agreement (avg $R^2 = 0.95 \pm 0.02$) with data analysed manually in the 1150 – 1600 cm^{-1} region of the IR spectrum for all IR active species. Supporting GC-FID measurements of CH_3CHO and CH_3OH were also in good agreement with those determined using the FTIR fitting algorithm in experiments P9 – P12 ([GC]:[FTIR] = (0.97 ± 0.03) and (1.05 ± 0.09), respectively).

Measurements of O_3 using commercial UV absorption analysers are not without uncertainty. Previous laboratory studies have shown an interference in O_3 measurements when a commercial trace O_3 analyser was exposed to high concentrations (>1 ppm) of low-volatility aromatics (Kleindienst et al., 1993). Whilst no aromatics were present in our system, it is possible that carbonyls and RO_2 radicals with cross-sections ~10^{-19} cm^2 $molecule^{-1}$ (λ = 254 nm) could be a potential interference. The TEC 49C model analyser used here measures an I_0 signal after passing the gas sample through an O_3 scrubber. If a potential interfering species could partially pass the O_3 scrubber system unharmed, a falsely low I_0 would be recorded, leading to an underestimation in $[O_3]$. Prior to each experiment, the $[O_3]$ was monitored upon sequential introduction of each reactant into the HIRAC chamber and no interference signal was observed before photolysis. Similarly, once the photolysis lamps were turned off, a slow decay in $[O_3]$ was observed, consistent with the combination of the characterised wall loss and chamber dilution rate, suggesting that any potential interference signal was unlikely a reactive intermediate (i.e. peroxy radical). Supporting evidence was obtained by the excellent agreement between the measured and modelled O_3 and $CH_3C(O)OH$ from R5b, where the two products were detected simultaneously using different techniques and under different radical loadings based on $j(Cl_2)$ and $[CH_3OH]_0$:$[CH_3CHO]_0$.

Recent studies have highlighted interferences in some FAGE based OH measurements (Mao et al., 2012;Novelli et al., 2014), typically involving sampling from systems containing high concentrations of O_3 and alkenes, with evidence presented consistent with the interference being due to the decomposition of stabilised Criegee intermediates. The system presented here does not contain an unsaturated hydrocarbons, however there was potential for a significant OH yield from the reaction of CH_3CO radicals with O_2 at low pressures inside the long inlet of the FAGE instrument (R1). Carr et al. (2011) and other workers (see references in Carr et al.) have shown that, at pressures < 350 mbar, the yield of OH from this reaction can become significant (<0.1) up to a yield of ~1 at very low pressures (~5 mbar).

$CH_3CO + O_2 \rightarrow OH + CH_2CO_2$ (lactone) R1

The interfering OH could be created inside FAGE at three different stages, with a potential interference coming from a combination of all three channels: 1) CH_3CO radicals are sampled directly via the FAGE instrument from the chamber and then react with O_2 in the FAGE inlet as they travel towards the OH fluorescence cell, 2) Cl atoms and CH_3CHO precursor are sampled from the chamber into the FAGE inlet, reacting to create CH_3CO radicals, which then react with O_2 and 3) Cl_2 and CH_3CHO are sampled from the chamber and, upon irradiation of the gas sample with the OH probe laser at 308 nm, the Cl_2 is photolysed, producing Cl atoms which can react with CH_3CHO. Experiment P9 was selected as an example for scenarios 1 and 2 (highest $[Cl]_0 = 1.14 \times 10^7$ molecule cm^{-3}) and P3 was selected for scenario 3 (high $[Cl_2]_0 \approx 6.6 \times 10^{14}$ molecule cm^{-3}), and the starting conditions were entered into the chemical simulation based on FAGE operating conditions (~3.8 mbar, 298 K, 1.0 mm pinhole, 280 mm inlet length, 6 slm sample rate and assuming plug flow conditions in the FAGE inlet). In scenario 1, the predicted $[CH_3CO]_{ss} \approx 10^3$ molecule cm^{-3} in the HIRAC chamber, a steady state so low that sampling by FAGE would make this channel ineffective through dilution (1000 mbar to 3.8 mbar) and radical losses on the inlet pinhole. Considering scenario 2, the sampled [Cl] by the inlet could lead to significant OH production via reaction of Cl with acetaldehyde and R1. After ~3 ms, the time for the gas sample to reach the OH probe laser, the model predicted an additional [OH] at the probe region equivalent to $\sim 7 \times 10^5$ molecule cm^{-3} sampled by the FAGE inlet, only half the limit of detection for the FAGE instrument (1.6×10^6 molecule cm^{-3}) and therefore insignificant compared to the observed values. Therefore, OH interference from scenario 2 was likely negligible. Finally, to test experimentally for scenario 3, the FAGE instrument was activated at the start of each experiment, before Cl_2, CH_3CHO and CH_3OH were added sequentially, and no enhanced OH signal was observed before each photolysis experiment, ruling out any interference from the photolysis of Cl_2 by the OH probe laser. As all three scenarios were deemed to produce negligible interfering OH concentrations, confidence is improved in the OH yields and k_5 presented here.

S4. Outputs from GEOS-CHEM modelling

The following figures show the percentage change in OH (Fig. S6), O_3 (Fig. S7), NO (Fig. S8) and PAN (Fig. S9.)for three different scenarios:

a) The total rate coefficient for Reaction (R5) is kept constant, but the yields are changed. We compare the current yields with those where $\alpha_{(R5c)}$ (the OH channel) is set to zero and $\alpha_{(R5a)}$: $\alpha_{(R5b)}$ = 3.2 (i.e. consistent ratio to the current work). This comparison highlights the overall importance of the OH yield from Reaction (R5).

b) The yields for Reaction (R5) are taken from this work, but the overall rate coefficient is varied from the IUPAC recommendation of $k_{(R5)} = 1.4 \times 10^{-11}$ cm^3 molecule^{-1} s^{-1} to that of the current study, $k_{(R5)} = 2.4 \times 10^{-11}$ cm^3 molecule^{-1} s^{-1}.

c) The yield and rate coefficient from this study ($\alpha_{(R5a)}$: $\alpha_{(R5b)}$: $\alpha_{(R5c)}$ = 0.37:0.12:0.51, $k_{(R5)} = 2.4 \times 10^{-11}$ cm^3 molecule^{-1} s^{-1}) are compared with the recommended IUPAC yield and rate coefficient ($\alpha_{(R5a)}$: $\alpha_{(R5b)}$: $\alpha_{(R5c)}$ = 0.41:0.15:0.44, $k_{(R5)} = 1.4 \times 10^{-11}$ cm^3 molecule^{-1} s^{-1}).

(c) OH

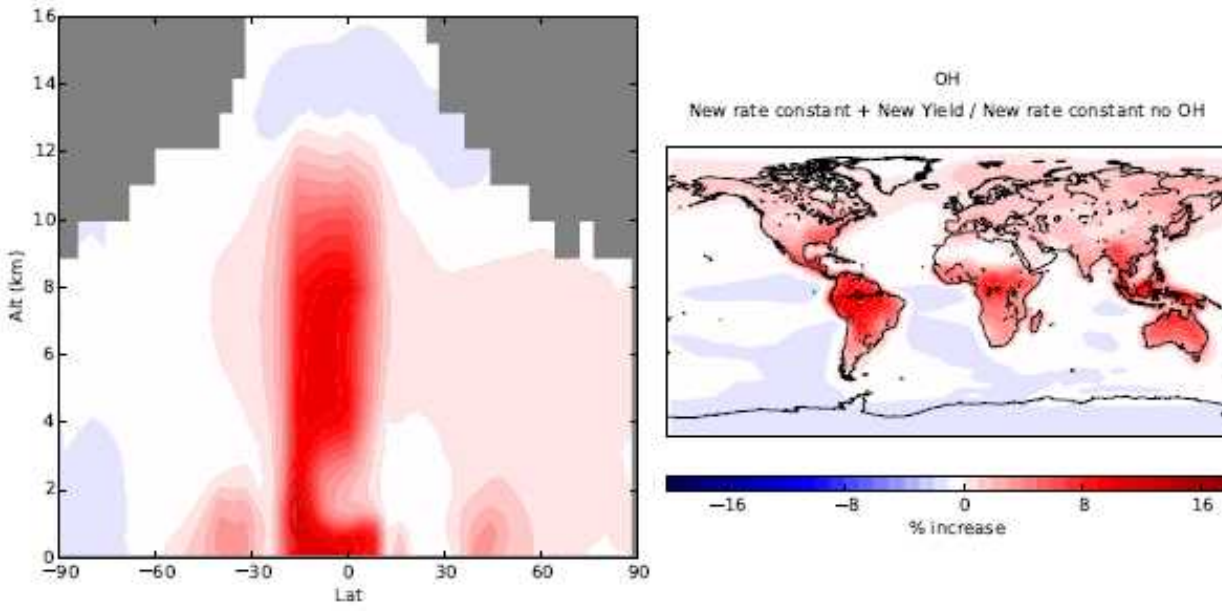

(b) OH

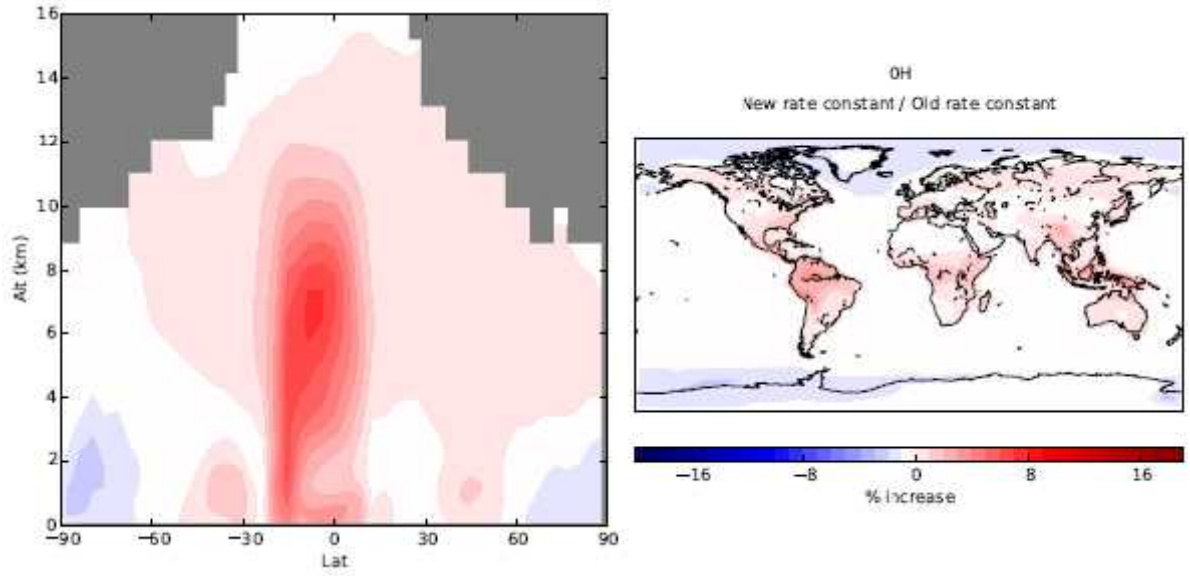

(c) OH

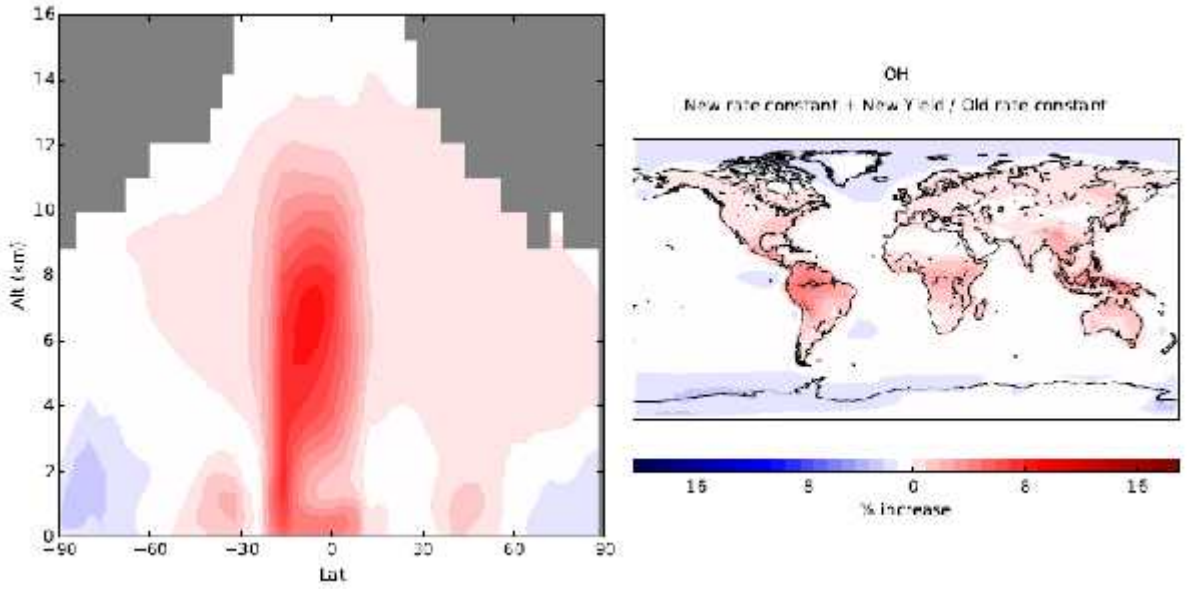

Fig. S6. Variation in calculated OH levels based on the three scenarios outlined above.

(a) O_3

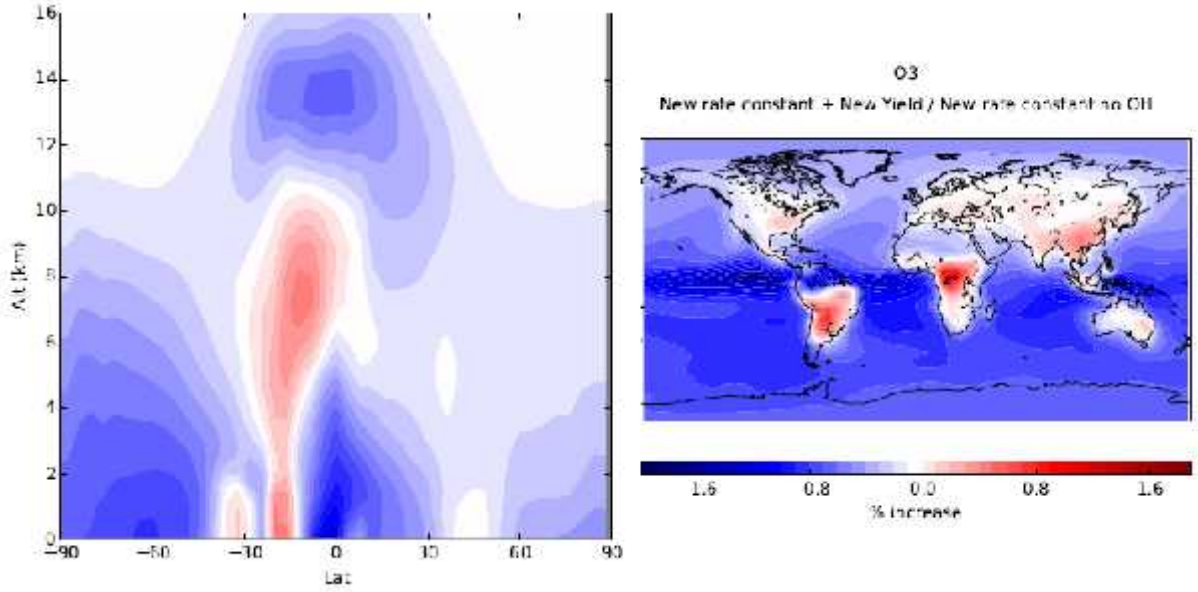
Alt (km)
Lat
O3
New rate constant + New Yield / New rate constant on OH
1.6
0.8
0.0
0.8
1.6
% increase

(b) O_3

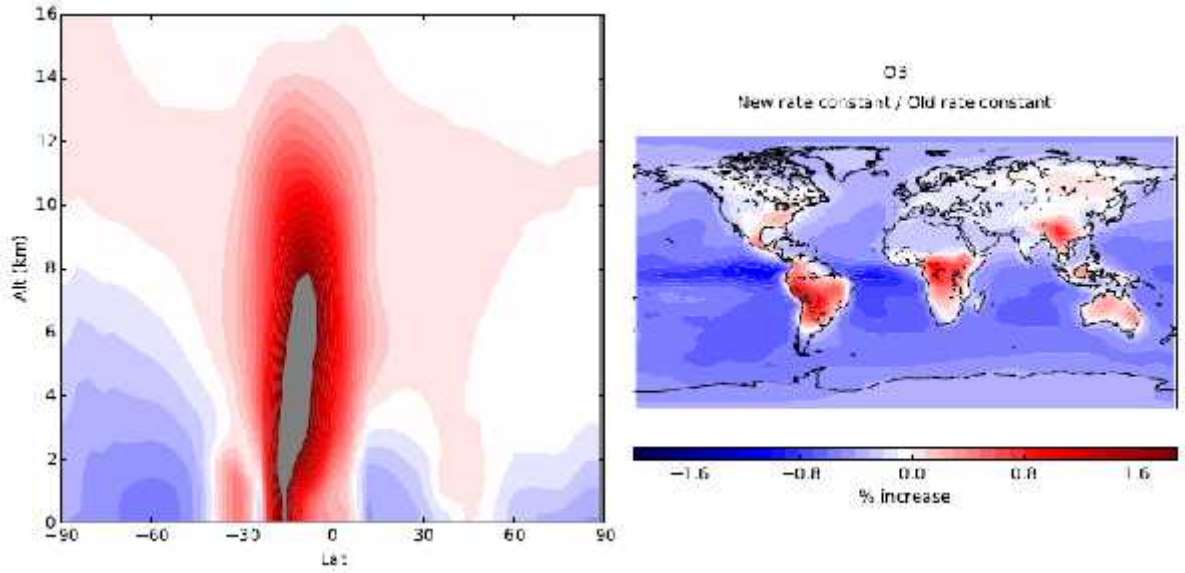
Alt (km)
Lat
O3
New rate constant / Old rate constant
% increase

(c) O_3

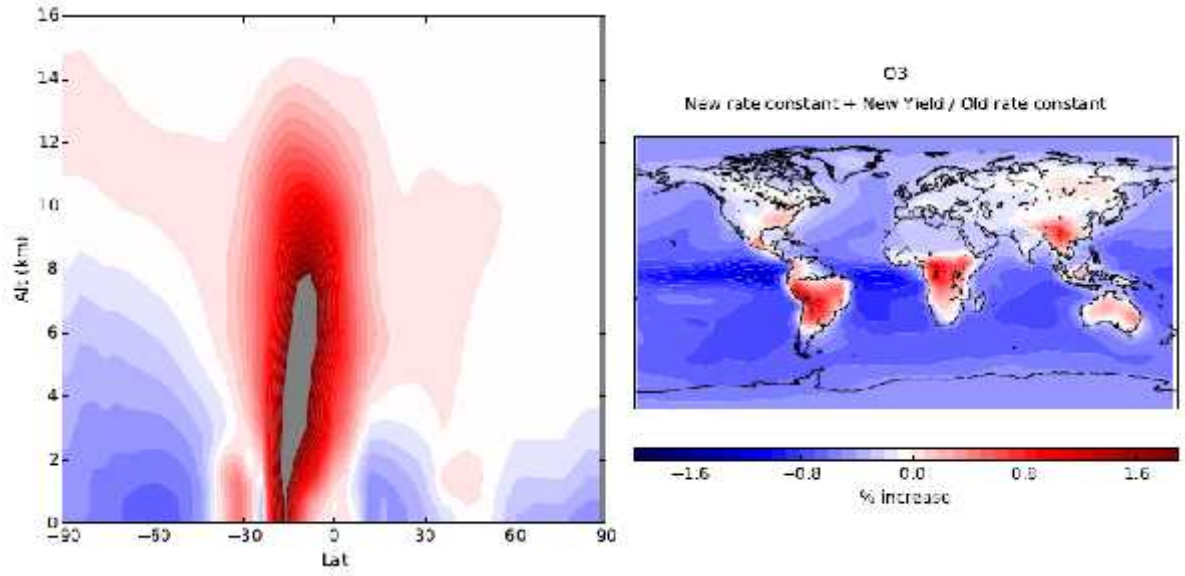

Fig. S7. Variation in calculated O_3 levels based on the three scenarios outlined above.

(a) NO

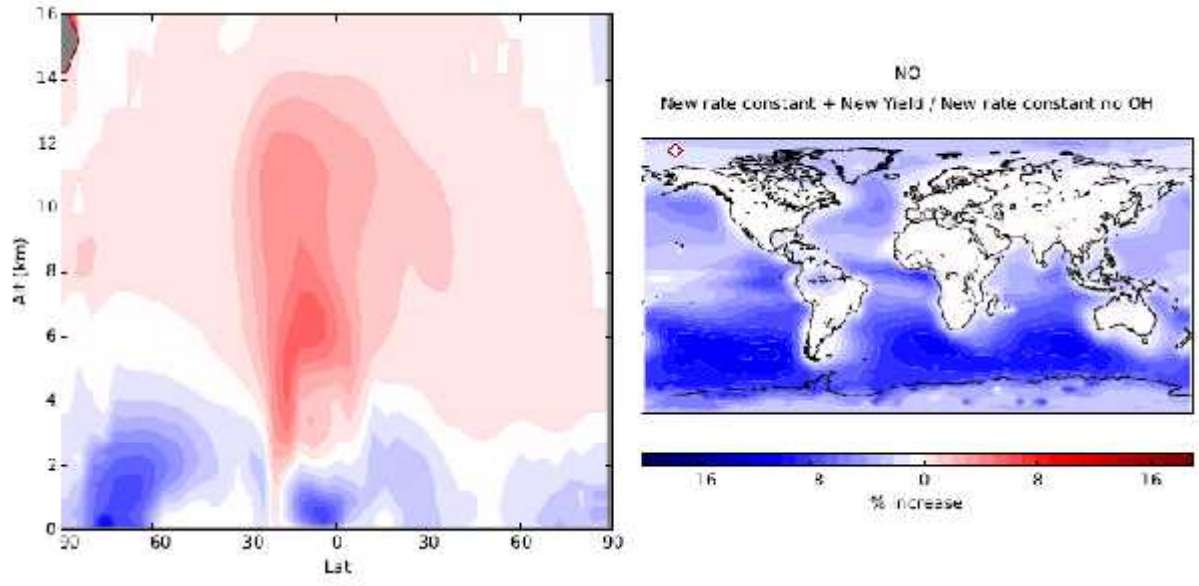

(b) NO

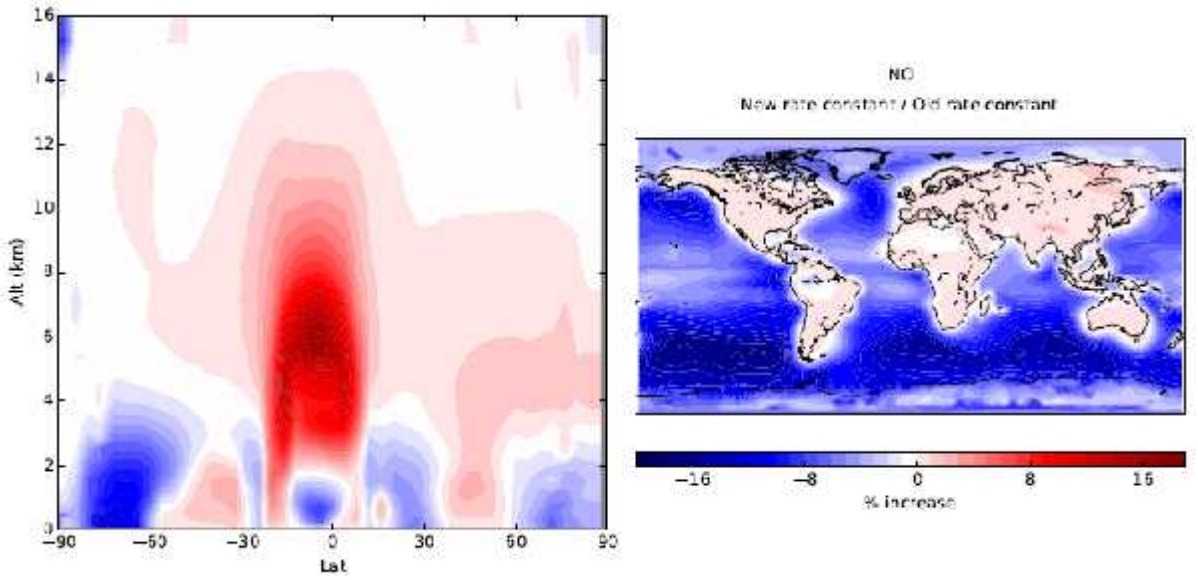

(c) NO

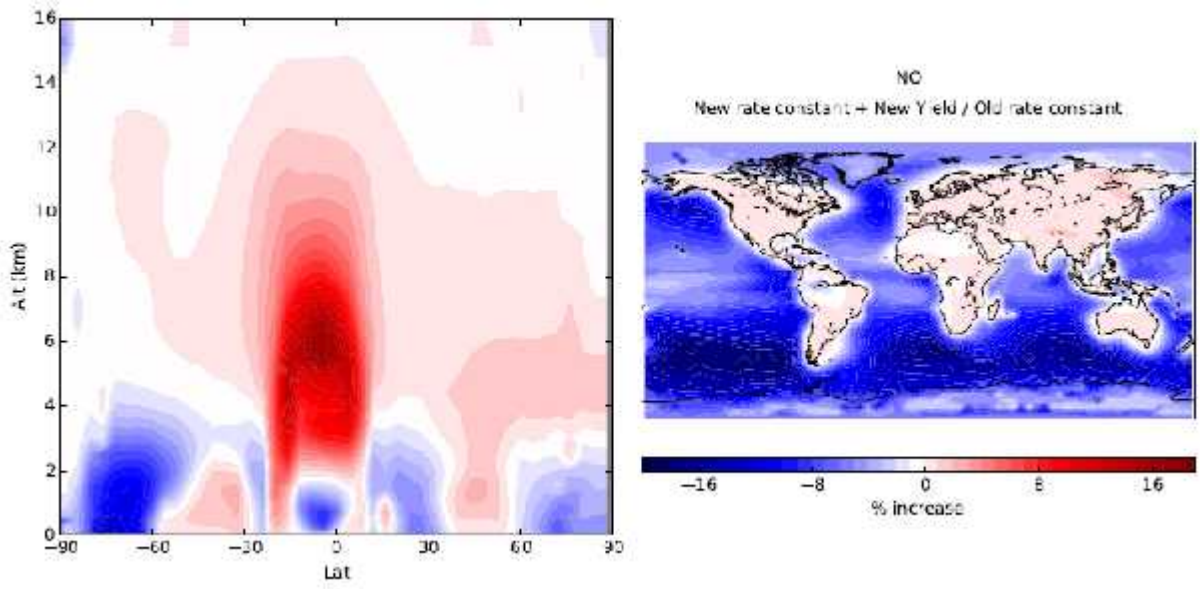

Fig. S8. Variation in calculated NO levels based on the three scenarios outlined above.

(a) PAN

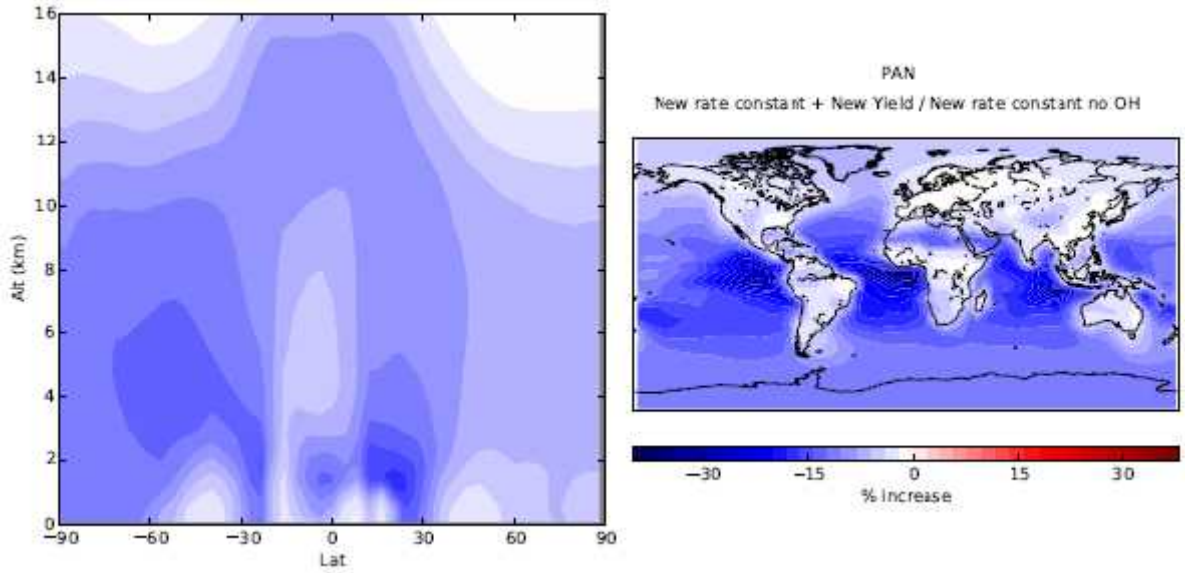
Alt (km)
Lat
PAN
New rate constant + New Yield / New rate constant no OH
% increase

(b) PAN

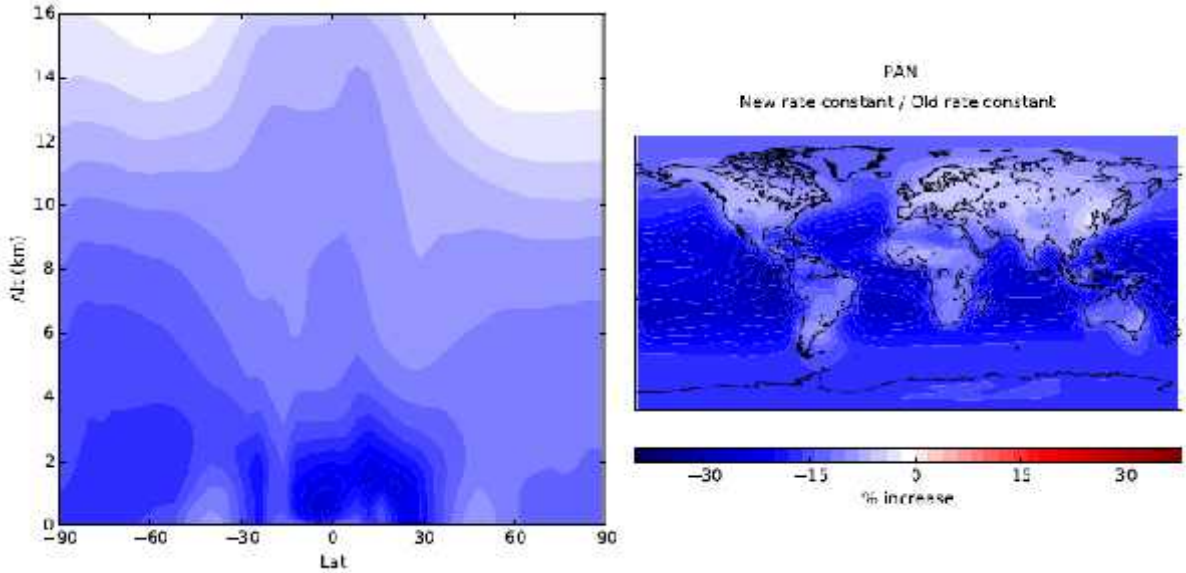
Alt (km)
Lat
PAN
New rate constant / Old rate constant
% increase

(c) PAN

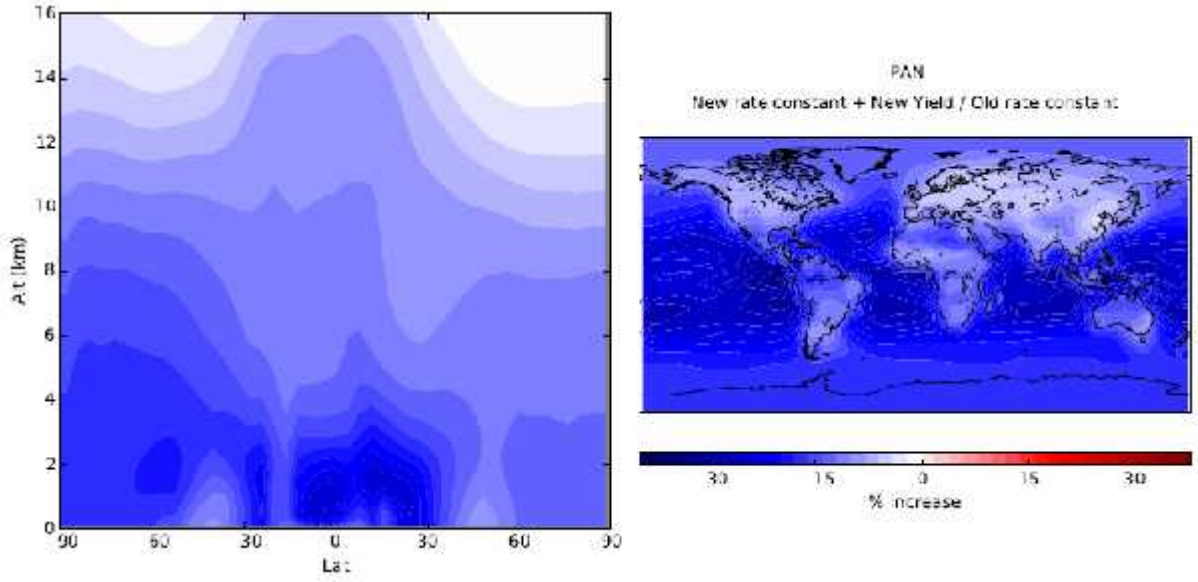

Fig. S9. Variation in calculated PAN levels based on the three scenarios outlined above.

References

Carr, S. A., Glowacki, D. R., Liang, C. H., Baeza-Romero, M. T., Blitz, M. A., Pilling, M. J., and Seakins, P. W.: Experimental and Modeling Studies of the Pressure and Temperature Dependences of the Kinetics and the OH Yields in the Acetyl + O_2 Reaction, J. Phys. Chem. A, 115, 1069-1085, 10.1021/jp1099199, 2011.

Kleindienst, T. E., Hudgens, E. E., Smith, D. F., McElroy, F. F., and Bufalini, J. J.: Comparison of Chemiluminescence and Ultraviolet Ozone Monitor Responses in the Presence of Humidity and Photochemical Pollutants, Journal of the Air & Waste Management Association, 43, 213-222, 1993.

Mao, J., Ren, X., Zhang, L., Van Duin, D. M., Cohen, R. C., Park, J. H., Goldstein, A. H., Paulot, F., Beaver, M. R., Crounse, J. D., Wennberg, P. O., DiGangi, J. P., Henry, S. B., Keutsch, F. N., Park, C., Schade, G. W., Wolfe, G. M., Thornton, J. A., and Brune, W. H.: Insights into hydroxyl measurements and atmospheric oxidation in a California forest, Atmos. Chem. Phys., 12, 8009-8020, 10.5194/acp-12-8009-2012, 2012.

Novelli, A., Hens, K., Ernest, C. T., Kubistin, D., Regelin, E., Elste, T., Plass-Dulmer, C., Martinez, M., Lelieveld, J., and Harder, H.: Characterisation of an inlet pre-injector laser-induced fluorescence instrument for the measurement of atmospheric hydroxyl radicals, Atmos. Meas. Tech., 7, 3413-3430, 10.5194/amt-7-3413-2014, 2014.

Orlando, J. J., Tyndall, G. S., Vereecken, L., and Peeters, J.: The atmospheric chemistry of the acetonoxy radical, J. Phys. Chem. A, 104, 11578-11588, 10.1021/Jp0026991, 2000.